ON THE SPECTRA OF HIGHLY-IONIZED KRYPTON, STRONTIUM, ZIRCONIUM AND RHODIUM EXCITED IN THE PLASMA OF THE TFR TOKAMAK

TFR GROUP

and

J.F. WYART
Laboratoire Aimé Cotton, CNRS II Campus Universitaire
91405 - Orsay (France)

Février 1987

ON THE SPECTRA OF HIGHLY-IONIZED KRYPTON, STRONTIUM, ZIRCONIUM AND RHODIUM EXCITED IN THE PLASMA OF THE TFR TOKAMAK

TFR GROUP

Association Euratom-CEA
Département de Recherche sur la Fusion Contrôlée
CEN-CADARACHE
13108 - ST PAUL LEZ DURANCE Cédex 1 (France)

and

J.F. WYART

Laboratoire Aimé Cotton, CNRS II*
Campus Universitaire
91405 - ORSAY (France)

ABSTRACT

Strontium, zirconium and rhodium have been injected into TFR tokamak plasmas by using the laser blow-off technique, and their spectra recorded either photographically (Zr, 10-92 Å) or photoelectrically (all three elements, 10-330 Å). Line identifications for several isoelectronic sequences from sodium -like to gallium- like are reported. Additionally, isoelectronic regularities observed for these three elements have allowed to identify a few krypton lines left unidentified in our previous work [1].

---

* In Association with Paris-Sud University

1. INTRODUCTION

Multicharged ions of high-Z_N elements are many electron systems with complex emission spectra which have been identified only in few cases, in the vicinity of simple isoelectronic sequences. These ions can be produced in laboratory plasmas with widely different electron densities : laser-produced plasmas, vacuum sparks, and tokamak discharges. This last case, as a consequence of plasma conditions close to corona equilibrium, has a specific interest. In particular, optical transitions between excited levels (which in laser-produced plasma spectra may be as intense as transitions to the ground state) are not a dominant feature in tokamak plasma spectra. Additionally, the presence of intrinsic impurities from the walls and/or the current aperture limiter has a two fold consequence : i) it provides standards for wavelength calibration, and ii) it masks the lines of the element under study in the dense spectral region of $n = 2, \Delta n = 0$ transitions of Fe, Cr, and Ni.

Systematic investigations of heavy ion spectra had been undertaken on the TFR tokamak, starting with the rare gas spectra of krypton [1] and xenon [2]. The analysis of krypton spectra led to the identificaiton of 48 lines in the isoelectronic sequences of potassium, argon, aluminum, magnesium, sodium, fluorine and oxygen, but left many lines unidentified. To extend this uncompleted work, it is necessary to use isoelectronic regularities, thus prompting us to study neighbouring elements. The spectra of strontium, zirconium and rhodium (injected by the laser blow-off technique [3, 4]) have been recorded either photographically (Zr, 10-92 Å) or photoelectrically (all three elements, up to 330 Å). The interpretation of these additional spectroscopic data (along with supplementary identification of Kr lines) will be reported in this paper. Independently, the study of the same isoelectronic sequences (in the same wavelength range) has also progressed from observations on the PLT and TFTR tokamaks [5-7].

2. EXPERIMENTAL CONDITIONS

The experiments reported in this paper have been performed on ohmically heated TFR tokamak plasmas. Zr spectra were photographically recorded in the 10-92 Å range by using a 2 m, grazing incidence (1.5°) Schwob-Fraenkel spectrograph [8, 9], equipped with a 2400 groove mm^{-1}, gold coated, 1° blaze, Bausch and Lomb grating. A Zr puff was injected by the laser blow-off technique into a quasi-steady He plasma, having the following parameters : plasma current I_p = 200 kA, toroidal magnetic field B_T = 4 T, graphite limiter radius a = 19.5 cm, central electron density $n_e(0)$ = 9. x 10^{13} cm^{-3}, and central electron temperature $T_e(0)$ = 1.4 keV. The injected atoms, firstly ionized at the plasma periphery, typically reach the plasma center after 10 ms, their maximum ionization degree depending on the $T_e(0)$ value. Helium was used as the filling gas because the injected ions life time increases with the atomic mass of the base ions [10, 11], being of the order of 100 ms for the central ions in these experiments. A fast shutter in front of the spectrograph input slit was only opened during ~ 200 ms starting from the injection time, in order to increase the contrast between Zr lines and intrinsic element (C, O, Fe, Cr and Ni) lines. Sufficient plate exposure needed ~ 100 discharges to be recorded.

The grazing incidence spectrograph has been recently transformed by J.L. Schwob into a multichannel spectrometer by equipping it with a multichannel detector (adjusted on the Rowland circle by using an interferometric technique) movable along the Rowland circle. The detector consists of a MgF_2 coated, funneled microchannel plate (MCP), associated with a phosphor screen image intensifier and coupled by a flexible fiber optic conduit to a 1024 element photodiode array (controlled and read-out by a commercially available PAR-1461 EGG Princeton Applied Research optical multichannel analyser system). An identical system, installed on the Princeton PLT and TFTR tokamaks, has been described by Schwob et al [12]. With a 600 groove mm^{-1} Jobin-Yvon holographic grating the total spectral range of the instrument is 10-330 Å, with a ~ 0.2 Å (full width at half maximum) spectral resolution. The MCP spectral range per shot varies from 15 Å at the short wavelength limit (10 Å) to 70 Å at the long wavelength limit (330 Å). Sr, Zr and Rh have been injected into ohmic hydrogen plasmas having the following parameters : I_p = 200 kA, B_T = 4.5 T, a = 20 cm, $n_e(0)$ = 8 x 10^{13} cm^{-3} and $T_e(0)$ = 1.3 - 1.5 keV. The spectrometer was operated in the spectral mode with 20 ms exposure (read-out) time ; as a consequence, only 3 spectra with important injected impurity ion lines

(with respect to intrinsic impurity lines) were available. Line identification is based on an average of these 3 spectra, on a single shot basis. A complete spectrum over the total accessible spectral range is obtained by displacing the microchannel plate carriage in between shots. Eight to nine discharges are sufficient to cover completely the 10 Å to 330 Å region (to be compared with the 100 discharges necessary with the spectrograph to obtain a photographic spectrum). Figures 1 and 2 (referring to Sr and Zr injection, respectively) show, for a given MCP position along the Rowland circle (different in the two figures) two spectra, the lower ones being taken just before the injection time. The wavelength scale (upper abscissa) has been obtained in the way discussed in the following section. For both figures we have pointed the most intense identified Zr ans Sr lines, along with the strong intrinsic impurity lines (appearing alone in the lower spectra).

3. PROCEDURE FOR LINE WAVELENGTH CALIBRATION

The wavelengths of known intrinsic impurity (C, N, O, Cr, Fe and Ni) lines have been used as internal standards. For the first three elements there is no major problem and we have taken the wavelength values from Kelly [13]. However, for heavy elements (such as Cr, Fe and Ni) there is no unanimous agreement on the exact experimental wavelength values ; of course, this limits the experimental accuracy of the newly classified lines when intrinsic impurity lines are used as wavelength standards (see, e.g., the discussion by Hinnov et al [7]). We have therefore relied on the assessement works from Culham Laboratory for the F-like to Li-like sequences [14], and from the National Bureau of Standards for less ionized ions [15-17].

For the photographic spectra the standard procedure of wavelength determination by polinomial fitting has been used, the spectra obtained on plasmas without Zr injection helping in the identification of Zr lines. The estimated accuracy of the wavelength measurements is between 0.01 Å and 0.02 Å, depending on the intensity and profile of the line under study.

The problem is much more complicated in the case of photoelectric detection, since the MCP is tangent to the Rowland circle (being thus coincident with it at only one point) and moreover a fiber optic taper is required. Wavelength calibration of the spectrometer is based on the grating equation and geometrical computations. The first step is to establish the relationship between the pixel number p along the linear PhotoDiode Array (PDA) and the corresponding wavelength λ, for a given position y of the MCP carriage on the Rowland circle. Following the grating equation and using the spectrometer geometry (schematically shown in figure 3), one obtains :

$$k\lambda_{\text{Å}} = \frac{10^7}{N}\left\{\cos\alpha - \cos\left[\beta_0 + \operatorname{arccotg}\left(\cot\beta_0 + \frac{Rn}{(p-p_0)M}\right)\right]\right\} \qquad (1)$$

where k is the diffraction order, N the grating groove density per mm, α the grazing incidence angle, R the Rowland circle diameter, n the number of pixel per unit length on the PDA, M the fiber optic taper magnification (1.75 for our system) and p_0 the number of the central pixel corresponding to the middle of the MCP. β_0, the diffraction angle for the central pixel, is given by :

$$(y_c - y)^2 = l^2 + (\frac{R}{2} + h)^2 - 2l(\frac{R}{2} + h)\cos\left[2(\frac{x_L - x_S}{R} - \beta_o)\right] \quad (2)$$

where l is the distance JO between the lead screw swivel joint center and the center of the Rowland circle, h the distance HN from the nut pivot to the Rowland circle, x_L and x_S the lengths of the arcs GL and SH, and y_c a calibration factor for the carriage position.

The validity of this calibration was checked using the known lines of intrinsic impurities in TFR. It was found that the geometric relationship (2) needs the addition of an empirical small correction factor $\Delta y_c(y)$, function of the screw position y, in order for the predicted and measured value of the wavelength λ_o corresponding to the central pixel p_o to coincide. The results of this calibration procedure are shown in figure 4a, where the difference $\Delta\lambda$ between computed and known wavelengths of intrinsic impurity lines (for a given y position of the MCP) is plotted as a function of pixel number (lower abscissa scale) and computed wavelength (upper abscissa scale). The vertical bars have a height equal to two pixel widths on the wavelength scale (thus implying a precision of ± 1 pixel in the line peak localisation). Figure 4a indicates that the precision of the computed λ's as function of p (including the geometrical correction Δy_c) is quite good in the central region of the PDA, between approximately pixels 300 and 800. However, as one approaches the PDA edges, on both sides, a discrepancy in wavelength appears increasing gradually towards the edge. Since the shape of this discrepancy does not depend on the position y of the MCP along the Rowland circle, this effect has been attributed to image distortion in the fiber optic chain. Consequently en empirical corrective term $\Delta M(p)$, function of p, has been introduced into equation (1), thus permitting to obtain the same accuracy in wavelength measurement over the entire pixel domain, for any y position (figure 4b). With the 600 groove mm^{-1} grating, the estimated accuracy of the wavelength values quoted in section 4 are of ± 0.05 Å (i.e., of the order of the error bar hights in figure 4, corresponding to an uncertainty of ± 1 pixel). This is a pessimistic estimate for strong lines, the maximum of which can be located to better than ± 1 pixel.

4. DATA INTERPRETATION

Some of the ions present in the investigated spectra belong to isoelectronic sequences which have already been studied by means of the relativistic multiconfigurational Dirac-Fock method [18], or the relativistic parametric potential method [19, 20], up to very high ionization stages (for example, in the aluminum and silicon sequences [21-23]). We used these results and also some unpublished calculations by the second method.

The analysed isoelectronic sequences will be described below, by order of increasing electron number in the sequence. It is recalled that five $n = 2$, $\Delta n = 0$ transitions of F-like Kr XXVIII and O-like Kr XXIX had been found in the first step of our work [1], but none of the same transitions has been firmly identified in our Sr, Zr, and Rh spectra, Na-like ions being those of highest charge emitting in the observed spectral range.

4.1 Sodium isoelectronic sequence

Four of five lines of Sr XXVIII observed in laser-produced plasmas [24] and a few predicted by semi-empirical methods in Zr XXX [25] are present in our spectra ; as expected the 3p - 3s transitions to the ground state are much stronger than the 3d - 3p transitions.

4.2 Magnesium isoelectronic sequence

The presence of magnesium like Sr and Zr ions is revealed by the resonance line $3s^2\ {}^1S_0$ - $3s3p\ {}^1P_1$, already identified in laser-produced plasmas. It is seen that, as in sodium -like ions, the strongest $n = 3$, $\Delta n = 0$ transitions connecting excited energy levels are much weaker than in laser-produced plasmas.

The magnesium like spectrum of krypton had been analyzed without the support of extended ab initio predictions, the early work by Cheng and Johnson [26] being applied to few elements in this sequence. Systematic investigations by means of the relativistic parametric potential method contributed recently to the identification of 40 lines in a laser-produced plasma Sr spectrum obtained at the GRECO-ILM laser facility [27]. The energy levels and transition probabilities within all six configurations with two $n = 3$ electrons and the 3s4s and 3s4p upper configurations have been determined by means of the RELAC code [28].

The parameters describing the central potential were fitted to minimize the total energy of the $3s^2$ ground state and the same convergence criteria, applied to 27 ions in the sequence Ti XI-Xe XLIII, led to a good isoelectronic consistency of these independent results. The systematic discrepancies between theoretical and experimental energies are a smooth function of atomic number and all, but one, previously reported Kr XXV levels are confirmed. The $3s3d\ ^3D_2$ level was built from two transitions towards $3s3p\ ^3P_1$ (129.895 Å) and $3s3p\ ^3P_2$ (144.665 Å), with nearly equal intensities. From present theoretical predictions, the branching ration of these transitions should be 4 to 1 in favour of the $^3D_2$-$^3P_1$ decay, and the regularity of the energy discrepancies requires that the wavelength of this transition be lowered by 0.6 Å. Consequently, the identification of the two lines in [1] should be cancelled and replaced by the previously unidentified line at 129.36 Å (with energies in cm^{-1} 1185320 $^3D_2$ - 412286 $^3P_1$). Finally, among weak Sr and Zr lines, two could be traced to the $3p^2\ ^3P_2$ - $3s3p\ ^3P_2$ decay in Sr XXVII and Zr XXIX.

All lines presently observed in the sodium and magnesium sequences are listed in table I. Note that the electron temperature is too low to observe the strong $\Delta n = 0$ transitions of Na-like Rh XXXV and Mg-like Rh XXXIV, even if weak lines are effectively found in the Rh spectrum near the predicted wavelengths.

4.3 Aluminum isoelectronic sequence

This isoelectronic sequence has already been identified in many elements, including Zr[5, 7], Kr[1], and Ag[6]. Interpolations for Sr led to the identification of several lines. Our wavelength measurements are more accurate in Zr than those of Finkenthal et al [5], and agree with the improved values reported by Hinnov et al [7]. Two lines have been added to the Kr XXIV line list, one of them being a blend of the two transitions $3s^23p\ ^2P_{1/2}$ - $3s3p^2\ ^2S_{1/2}$ and $3s^23p\ ^2P_{3/2}$ - $3s3p^2\ ^2P_{1/2}$, which have nearly equal wavelengths for a wide range of ions. Table II list our identifications.

4.4 Silicon isoelectronic sequence

The $3s^23p^k$ - $3s3p^{k+1}$ + $3s^23p^{k-1}3d$ transition arrays of ions isoelectronic with Al, Si, P, S and Cl overlap in multicharged ions ; consequenctly, so far only the simplest ones at both ends of the period have been investigated for nuclear

charges larger than 15. Recently, Huang has evaluated systematically the energies and transition probabilities for three low-lying configurations and all charge states of Si-like ions [23]. A comparison of the theoretical energy levels involved in the strongest transitions with their experimental values in the iron group elements led us to extrapolate the energy discrepancies in Kr, Sr and Zr. Some of the identified lines in Kr XXIII, Sr XXV and Zr XXVII are blended with intrinsic impurities (unfortunately, all for Sr XXV), as detailed in Table III.

4.5 Argon and chlorine isoelectronic sequences

The intense resonance line of argon-like ions, $3p^6\ {}^1S_0$ - $3p^53d\ {}^1P_1$, dominates the array of $n = 3$, $\Delta n = 0$ transitions, and was easily identified in all three elements. For the same reason, the presence of the Cl-like Kr XX lines was already proved in our krypton spectra [1]. By combining recent experimental results [6, 7] and theoretical evaluations of energies and transition probabilities by means of the multiconfiguration Dirac-Fock method, four Cl-like lines have been traced so far in Kr XX, Sr XXII and Zr XXIV. According to Huang et al [29], level crossing occurs for the $3p^4(^3P)3d\ {}^2D_{5/2}$ and $3p^4(^1S)3d\ {}^2D_{5/2}$ levels ; consequently, the behaviour of the strongest lines for increasing atomic mass is irregular. Some ions (Zr^{23+} and Rh^{28+}) have not been considered by Huang et al [29], thus hampering the comparison between experiment and theory ; more theoretical work will be needed in order to extend these preliminary results. Table IV lists the line wavelengths for these two sequences.

4.6 Potassium isoelectronic sequence

We had already identified seven Kr XVIII lines as $3p^63d$ - $3p^53d^2$ transitions [1] ; a new line (at 99.67 Å) has been recently identified (table V). The strongest of these transitions have also been found in the spectra of Sr XX, Zr XXII and Rh XXVII (Table V). This isoelectronic sequence has a smooth behaviour for increasing atomic mass.

4.7 Lower charge ions

They are, of course, present in TFR plasmas, but the strong resonance lines of Kr, Zr and Sr occur at wavelengths larger than 300 Å. In Rh the copper-like and zink-like $n = 4$, $\Delta n = 0$ transitions are important features of the observed spectrum and some weaker lines may be attributed to gallium-like Rh XV. All

these lines have already been observed in high vacuum spark spectra with better spectral resolution. The identified lines are listed in table VI.

5. CONCLUSION

Strontium, zirconium and rhodium have been injected into TFR tokamak plasmas ($n_e(0) \simeq 8 \times 10^{13}$ cm^{-3}, $T_e(0) \simeq 1.4$ keV)) by using the laser blow-off technique, and their spectra between 10 Å and 330 Å recorded photoelectrically. In addition, higher spectral resolution spectra of Zr have also been photographically recorded in the 10 - 92 Å range. Many spectral lines, belonging to several isoelectronic sequences, of these injected elements have been identified and listed in the tables. In addition, using isoelectronic sequence regularities, these new identifications have also allowed some Kr lines left unidentified in our previous work [1] to be identified. Further identification work (especially for weak kines, or lines blended with intrinsic impurity emission) is still in progress.

REFERENCES

[1] WYART, J.F. and TFR GROUP, Physica Scripta 31, 539 (1985)

[2] WYART, J.F., BAUCHE-ARNOULT, C., LUC-KOENIG, E. and TFR GROUP, Physica Scripta 32, 103 (1985)

[3] MARMAR, E.S., CECCHI, J.L. and COHEN S.A., Rev. Sci. Instrum. 46, 1149 (1975)

[4] BRETON, C., DEMICHELIS, C., HECQ, W. and MATTIOLI, M., Rev. Phys. Appliquée 15, 1193 (1980)

[5] FINKENTHAL, M., STRATTON, B.C., MOOS, H.W., HODGE, W.L., SUCKEWER, S., COHEN, S., MANDELBAUM, P. and KLAPISCH, M., J. Phys. B : At. Molec. Phys. 18, 4393 (1985)

[6] SCHWOB, J.L., WOUTERS, A. SUCKEWER, S., COHEN, S.A., and FINKENTHAL, M., J. Opt. Soc. Am. B 2, 68 (1986)

[7] HINNOV, E., BOODY, F., COHEN, S., FELDMAN, U., HOSEA, J., SATO, K., SCHWOB, J.L., SUCKEWER, S. and WOUTERS, A., J. Opt. Soc. Am. B 3, 1288 (1986)

[8] BRETON, C., DEMICHELIS, C., FINKENTHAL, M. and MATTIOLI, M., J. Opt. Soc. Am. 69, 1652 (1979)

[9] TFR GROUP, DOYLE, J.G. and SCHWOB, J.L., J. Phys. B : At. Molec. Phys. 15, 813 (1982)

[10] MARMAR, E.S., RICE, J.E. and ALLEN, S.L., Phys. Rev. Letters 45, 2025 (1980)

[11] TFR GROUP, Phys. Letters 87A, 169 (1982)

[12] SCHWOB, J.L., WOUTERS, A.W., SUCKEWER, S. and FINKENTHAL, M., Princeton Plasma Physics Laboratory Report PPPL 2419 (1987), submitted to Rev. Scient. Instrum.

[13] KELLY, R.L. "Atomic and ionic spectral lines below 2000 Å (H through Ar)". Oak Ridge National Laboratory, Report ORNL-5922 (1982)

[14] LAWSON, K.D., PEACOCK, N.J. and STAMP, M.F., J. Phys. B : At. Molec. Phys. 14, 1929 (1981)

[15] WIESE, W.L. (ed.), "Spectroscopic data for iron", vol. 4 of Atomic Data for Fusion Research, Oak Ridge National Laboratory, Report ORNL - 6089/V4 (1985)

[16] CORLISS, Ch. and SUGAR, J., J. Phys. Chem. Ref. Data 10, 197 (1981)

[17] SUGAR, J. and CORLISS, Ch., J. Phys. Chem. Ref. Data 6, 317 (1977)

[18] DESCLAUX, J.P., Comput. Phys. Commun. 9, 31 (1975)

[19] LUC-KOENIG, E., Physica 62, 393 (1972)

[20] KLAPISCH, M., SCHWOB, J.L., FRAENKEL, B.S. and OREG, J., J. Opt. Soc. Am. 67, 148 (1977)

[21] FARRAG, A., LUC-KOENIG, E. and SINZELLE, J., At. Dat. Nucl. Dat. Tables 27, 540 (1982)

[22] HUANG, K.N., At. Dat. Nucl. Dat. Tables 34, 1 (1986)

[23] HUANG, K.N., At. Dat. Nucl. Dat. Tables 32, 503 (1986)

[24] READER, J., J. Opt. Soc. Am. B 3, 870 (1986)

[25] EDLEN, B., Physica Scripta 17, 565 (1978)

[26] CHENG, K.T. and JOHNSON, W.R., Phys. Rev. A 16, 263 (1977)

[27] WYART, J.F., GAUTHIER, J.C., GEINDRE, J.P., TRAGIN, N., MONIER, P., KLISNIK, A. and CARILLON A., accepted for publication in Physica Scripta.

[28] KLAPISCH, M., BAR-SHALOM, A. and LUC-KOENIG, E., (unpublished)

[29] HUANG, K.N., KIM, Y.K., CHENG, K.T. and DESCLAUX, J.P., At. Dat. Nucl. Dat. Tables 28, 355 (1983)

[30] READER, J., J. Opt. Soc. Am. 73, 796 (1983)

[31] HINNOV, E., in "Atomic physics of highly ionized atoms" (R. Marrus, ed.), Plenum : New York, 49 (1983)

[32] READER, J., ACQUISTA, N. and COOPER, D., J. Opt. Soc. Am. 73, 1765 (1983)

[33] ACQUISTA, N. and READER, J., J. Opt. Soc. Am. B 1, 649 (1984)

[34] READER, J. ACQUISTA, N. and GOLDSMITH, S., J. Opt. Soc. Am. B 3, 874 (1986)

FIGURES CAPTIONS

Fig. 1 - Photoelectric spectra with strontium injection between ~ 82 Å and ~ 94 Å. Lower spectrum : prior to injection ; upper spectrum : after injection.

Fig. 2 - Photoelectric spectra with zirconium injection between ~ 115 Å and 146 Å. Lower spectrum : prior to injection ; upper spectrum : after injection.

Fig. 3 - Schematic of geometry of grazing incidence (1.5°) Schwob-Fraenkel spectrometer equipped with multichannel plate (MCP) carriage. The nut pivot is attached to the carriage, which can be moved along the Rowland circle by rotation of the lead screw ; the swivel joint center J is fixed with respect to the spectrometer (courtesy of J.L. Schwob).

Fig. 4 - Difference $\Delta\lambda$ between computed wavelengths and experimental ones as function of pixel number along the PDA (lower abscissa) and computed wavelength (upper abscissa) for the MCP position y = 220 mm (corresponding to a wavelength of 102.48 Å for the central pixel). (a) without taper magnification correction $\Delta M(p)$, but with geometric correction $\Delta y_c(y)$; (b) with both corrections. Further details in the text.

TABLE I - Wavelength (Å) of sodium-like and magnesium-like strontium and zirconium lines

Transition			Sr XXVII-XXVIII		Zr XXIX-XXX	
even	-	odd	λ_{exp}	$\lambda_{(others)}$	λ_{exp}	$\lambda_{(others)}$
$3d\ ^2D_{3/2}$	-	$3p\ ^2P_{1/2}$		127.230[b]	115.08	115.091[d]
$3s3d\ ^3D_3$	-	$3s3p\ ^3P_2$	130.76	130.738[a]	f	121.141[a]
$3s3d\ ^1D_2$	-	$3s3p\ ^1P_1$	133.74	133.711[a]	123.27	123.250[a]
$3s^2\ ^1S_0$	-	$3s3p\ ^1P_1$	142.45	14[illegible]38[a]	128.48	128.479[a], 128.52[e]
$3d\ ^2D_{5/2}$	-	$3p\ ^2P_{3/2}$	147.53	147.567[b]	136.65	136.639[d]
$3p^2\ ^3P_2$	-	$3s3p\ ^3P_2$	149.24	149.27[c]	134.74	134.73[c]
$3d\ ^2D_{3/2}$	-	$3p\ ^2P_{3/2}$	153.53[g]	153.582[b]		
$3s\ ^2S_{1/2}$	-	$3p\ ^2P_{3/2}$	159.78	159.779[b]	142.83	142.799[d], 142.84[e]
$3s\ ^2S_{1/2}$	-	$3p\ ^2P_{1/2}$	203.64	203.664[b]		

(a) ref. [30] , (b) ref. [24] , (c) recent calculations [27] , (d) ref. [25], predictions,
(e) ref. [31] , (f) weaker than Fe XXI 121.21 Å, , (g) probable blending with Sr XXVI

TABLE II - Wavelength (Å) of aluminum-like krypton, strontium and zirconium lines

Transition	Kr XXIV		Sr XXVI		Zr XXVIII	
	λ_{th}[a]	λ_{exp}	λ_{th}[a]	λ_{exp}	λ_{th}[a]	λ_{exp}
$3s^23p\ ^2P_{1/2}$ - $3s^23d\ ^2D_{3/2}$	117.22	118.60[b]	105.96	107.00	95.68	96.61[f]
$3s^23p\ ^2P_{1/2}$ - $3s3p^2\ ^2P_{3/2}$	129.26	130.71[b]	114.84	116.23[c]	102.37	103.37[g]
$3s^23p\ ^2P_{1/2}$ - $3s3p^2\ ^2P_{1/2}$	131.18	132.44	115.90	d	102.42	103.56[g,l]
$3s^23p\ ^2P_{1/2}$ - $3s3p^2\ ^2S_{1/2}$	150.18	152.07[D]	135.64	137.19[D]	122.67	124.01[g,D]
$3s^23p\ ^2P_{1/2}$ - $3s3p^2\ ^2D_{3/2}$	171.66	172.48	152.76	153.53[i]	136.26	136.92[g]
$3s^23p\ ^2P_{3/2}$ - $3s^23d\ ^2D_{5/2}$	130.09	131.81[b]	120.07	121.50	111.19	112.47[g]
$3s^23p\ ^2P_{3/2}$ - $3s^23d\ ^2D_{3/2}$	132.27	134.10[b]	122.29	123.85	113.13	114.53[g]
$3s^23p\ ^2P_{3/2}$ - $3s3p^2\ ^2P_{3/2}$	147.79	149.79[b]	134.26	136.00[e]	122.60	124.01[g,D]
$3s^23p\ ^2P_{3/2}$ - $3s3p^2\ ^2P_{1/2}$	150.31	152.07[D]	135.72	137.19[D]	122.67	i
$3s^23p\ ^2P_{3/2}$ - $3s3p^2\ ^2D_{5/2}$	193.66	194.44	173.89	h	156.17	156.58[g]

(a) theoretical values from ref. [22] , (b) already interpreted in ref. [1] , (c) partial blending with Fe XXII 116.28 Å possible, (d) probably blended with Fe XXII 117.17 Å, (e) tentative, since near Fe XXII 135.78 Å , (f) blending with Zr XXVII, (g) present value, but already interpreted in ref. [7], (h) probably blended with Fe X 174.53 Å, (i) masked by two other strong Zr XXVIII transitions, (j) probable blending with Sr XXVIII, (l) doubtful, due to its low transition probability [22], (D) two transitions for one line

TABLE III - Wavelength (Å) of silicon-like krypton, strontium and zirconium lines

Transition	Kr XXIII		Sr XXV		Zr XXVII	
	λ_{th}[a]	λ_{exp}	λ_{th}[a]	λ_{exp}	λ_{th}[a]	λ_{exp}
$3s^23p^2$ - $3s^23p3d$						
$^3P_2$ - $^3D_3$	115.40	116.79	105.02	106.16[b]	95.74	96.61[e]
$^1D_2$ - $^1F_3$	117.06	118.79	108.51	109.95[c]	100.99	102.30[f]
$^3P_1$ - $^3P_2$	122.66	124.32	112.97		104.30	105.56
$^3P_2$ - $^1P_1$	142.61	144.66	129.58	131.50[d]	117.88	119.30

(a) theoretical values from ref. [23]
(b) tentative, since near the blending Ni XXIII - Ni XXII 106.03 Å,
(c) eventually blended with Fe XIX 109.95 Å
(d) eventually blended with Cr XX 131.50 Å,
(e) blended with Zr XXVIII
(f) tentative, since near Fe XXI 102.22 Å

TABLE IV - Wavelength (Å) of argon-like and chlorine-like krypton, strontium, zirconium and rhodium lines

Transition	Kr XIX	Sr XXI	Zr XXIII	Rh XXVIII
	λ_{exp}	λ_{exp}	λ_{exp}	λ_{exp}
$3p^6\ {}^1S_0$ - $3p^5 3d\ {}^1P_1$	96.26[a]	87.95	80.66[d]	65.65
	Kr XX	Sr XXII	Zr XXIV	Rh XXIX
	λ_{exp}	λ_{exp}	λ_{exp}	λ_{exp}
$3p^5$ - $3p^4 3d$				
$^2P_{3/2}$ - $(^3P)^2D_{5/2}$	99.34	90.75[D]		
$^2P_{3/2}$ - $(^1D)^2P_{3/2}$	99.67[b]	90.75[D]	82.78[d]	
$^2P_{3/2}$ - $(^1S)^2D_{5/2}$		91.23	83.41	67.65
$^2P_{1/2}$ - $(^3P)^2D_{3/2}$	100.24	91.70	84.14	
$^2P_{3/2}$ - $(^1D)^2S_{1/2}$	103.88	93.93[c]	85.37[d]	

(a) already interpreted in ref. [1],
(b) blended with Kr XVIII,
(c) blended with Fe XVIII 93.93 Å,
(d) improved measurements of lines already interpreted in ref. [5],
(D) two transitions for one line

TABLE V - Wavelength (Å) of potassium-like krypton, strontium, zirconium and rhodium lines

Transition	Kr XVIII	Sr XX	Zr XXII	Rh XXVII
	λ_{exp}	λ_{exp}	λ_{exp}	λ_{exp}
$3p^6 3d$ - $3p^5 3d^2$				
$^2D_{3/2}$ - $^2D_{3/2}$	92.225[a]	84.15	77.02[c]	62.65
$^2D_{5/2}$ - $^2P_{3/2}$	92.728[a]	84.65	77.39	62.95
$^2D_{5/2}$ - $^2D_{5/2}$	93.353[a]	85.30	78.30[c]	63.95
$^2D_{5/2}$ - $^2F_{7/2}$	99.67[b]	90.20	82.22	

(a) already interpreted in ref. [1],

(b) blended with Kr XX,

(c) improved measurement of lines already interpreted in ref. [5]

TABLE VI - Wavelength (Å) of copper-like, zink-like and gallium-like rhodium lines

Ion	Transition	λ_{exp}	$\lambda_{(others)}$[a]
Rh XVII	$4p\ ^2P_{1/2}$ - $5s\ ^2S_{1/2}$	84.77	84.742[c]
	$4p\ ^2P_{3/2}$ - $5s\ ^2S_{1/2}$	88.43	88.461[c]
	$4p\ ^2P_{1/2}$ - $4d\ ^2D_{3/2}$	195.81	195.868[c]
	$4p\ ^2P_{3/2}$ - $4d\ ^2D_{5/2}$	212.92	212.875[c]
	$4s\ ^2S_{1/2}$ - $4p\ ^2P_{3/2}$	300.84	300.876[c]
Rh XVI	$4s^2\ ^1S_0$ - $4s4p\ ^1P_1$	277.15	277.14[d]
Rh XV	$4s24p\ ^2P_{3/2}$ - $4s4p^2\ ^2P_{3/2}$	268.14	268.134[e]
	$4s24p\ ^2P_{3/2}$ - $4s4p^2\ ^2P_{1/2}$	273.4[b]	273.604[e]

(a) from laser-produced plasmas , (b) weak and wide, possibly two lines at 273.25 Å and 273.55 Å,
(c) ref. [32] , (d) ref. [33],
(e) ref. [34]

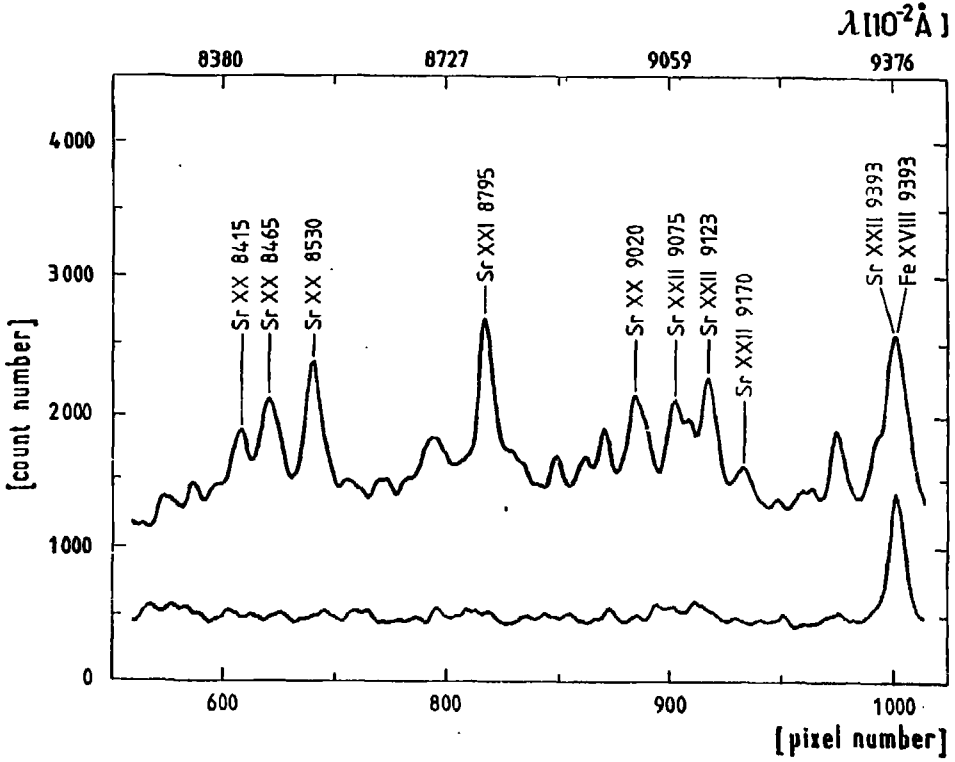
λ[10⁻²Å]
8380
8727
9059
9376
4000
3000
2000
1000
0
[count number]
Sr XX 8415
Sr XX 8465
Sr XX 8530
Sr XXI 8795
Sr XX 9020
Sr XXII 9075
Sr XXII 9123
Sr XXII 9170
Sr XXII 9393
Fe XVIII 9393
600
800
900
1000
[pixel number]

Figure 1

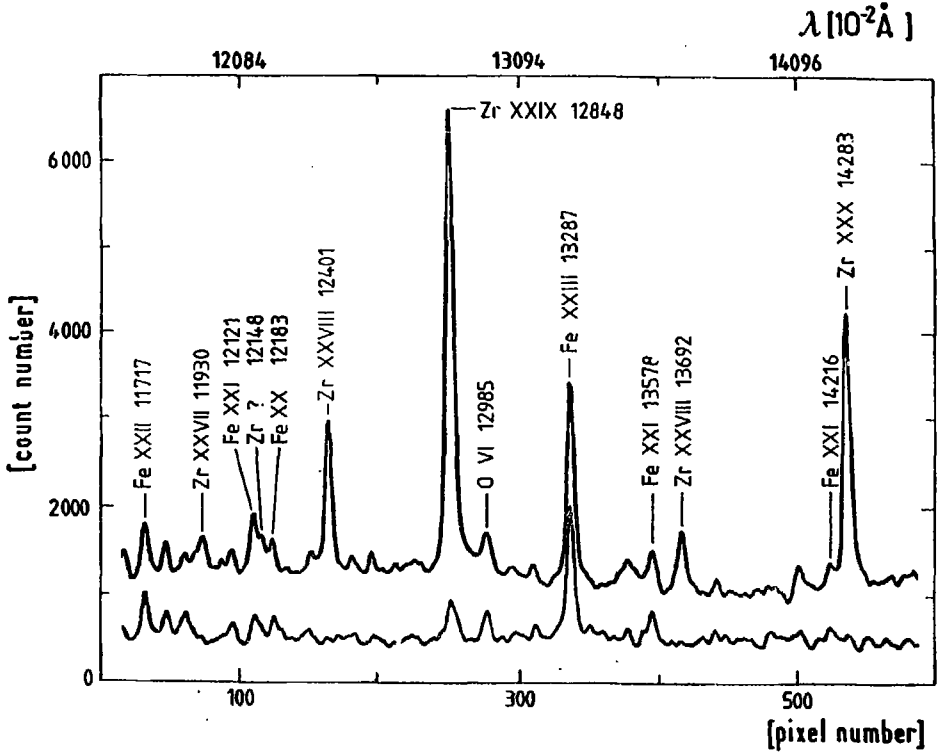
λ [10⁻²Å]
12084
13094
14096
Zr XXIX 12848
Fe XXII 11717
Zr XXVII 11930
Fe XXI 12121
Zr ? 12148
Fe XX 12183
Zr XXVIII 12401
O VI 12985
Fe XXIII 13287
Fe XXI 13578
Zr XXVIII 13692
Fe XXI 14216
Zr XXX 14283
[count number]
6000
4000
2000
0
100
300
500
[pixel number]

Figure 2

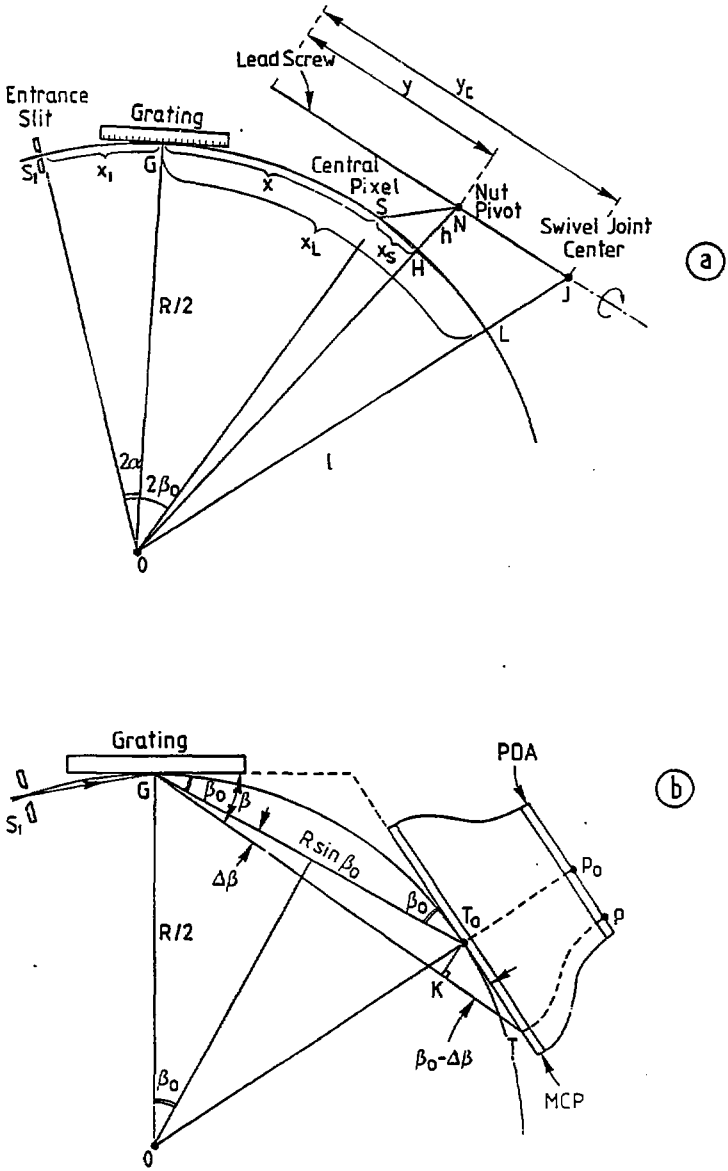
Lead Screw
y
y_c
Entrance Slit
Grating
S_1
x_1
G
x
Central Pixel
S
Nut Pivot
N
h
Swivel Joint Center
x_L
x_S
H
J
a
R/2
L
2α
$2\beta_o$
l
0
Grating
PDA
b
S_1
G
β_o
β
$R\sin\beta_o$
$\Delta\beta$
P_o
P
β_o
T_o
R/2
K
$\beta_o-\Delta\beta$
T
MCP
β_o
0

Figure 3

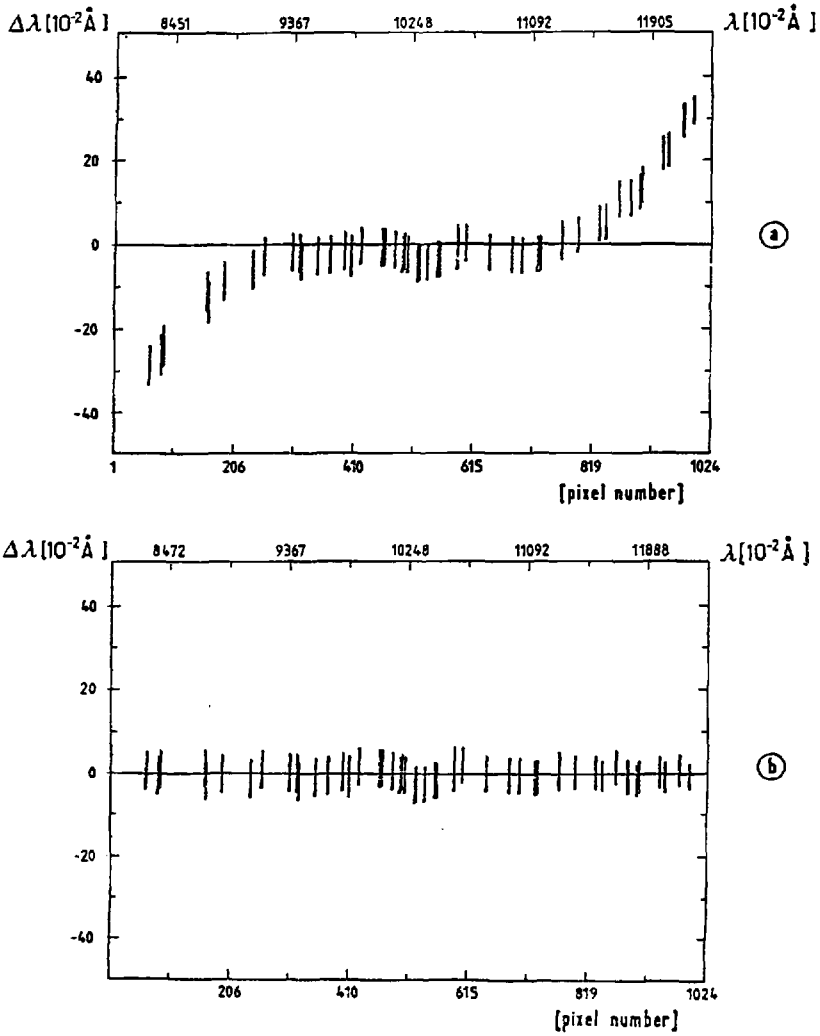
Δλ[10⁻²Å]
8451
9367
10248
11092
11905
λ[10⁻²Å]
40
20
0
-20
-40
1
206
410
615
819
1024
[pixel number]
a
Δλ[10⁻²Å]
8472
9367
10248
11092
11888
λ[10⁻²Å]
40
20
0
-20
-40
206
410
615
819
1024
[pixel number]
b

Figure 4

S C P

ÉQUIPE T.F.R.

LISTE N° 12 - MISE À JOUR DU 1ER. OCTOBRE 1985

EXPLOITATION PHYSIQUE DE L'EXPÉRIENCE

- COORDINATION.....	M. CHATELIER J. TACHON
- SECRÉTARIAT SCIENTIFIQUE.....	P. LECOUSTEY
- CONDUITE DE LA MACHINE.....	P. BANNELIER M. CHATELIER J. DUBOIS P. GIOVANNONI L. LAURENT
- MESURES MAGNÉTIQUES.....	P. LECOUSTEY
- INTERFÉROMÉTRIE HCN.....	D. VERON
- RÉFLECTOMÉTRIE.....	E. ANABITARTE F. SIMONET
- DIFFUSION THOMSON.....	J. LASALLE P. PLAIZ
- SPECTRES DE NEUTRES.....	J. HOTIER C. REVERDIN
- MESURES NUCLÉAIRES, X-DURS.....	A. GERAUD G. MARTIN
- RAYONS X-MOUS.....	L. JACQUET A.L. PECQUET
- SPECTROMÉTRIE (VISIBLE, UV, X-MOUS).....	C. BRETON C. DE MICHELIS M. HECQ M. MATTIOLI P. PLAIZ L. RAMETTE B. SACOTTC
- SPECTROMÉTRIE DE MASSE, CONDITIONNEMENT DES PAROIS, PLASMA PÉRIPHÉRIQUE, BOLOMÉTRIE.....	M.H. ACHARD A. GROSMAN F. LINET
- RAYONNEMENT CYCLOTRONIQUE ELECTRONIQUE A/ SPECTROMETRIE INFRAROUGE..... B/ ÉTUDES MICROONDES.....	L. LAURENT R. SOUBARAS B. ZANFAGNA
- MESURES DE LA TURBULENCE PAR DIFFUSION THOMSON.....	H. BARKLEY S. DE GENTILE J. GERVAIS J. OLIVAIN A. QUEMENEUR
- INJECTION DE GLACONS.....	H. DRAWIN A. GERAUD

./...

CHAUFFAGES ADDITIONNELS

- INJECTION DE NEUTRES..... J. DRUAUX
  M. FOIS
  P. GIOVANNONI
  J.P. ROUBIN

- CHAUFFAGE CYCLOTRONIQUE ELECTRONIQUE..... J.P. CRENN
  M. DUBOIS
  L. REBUFFI
  B. TOURNESAC
  M. TUSZEWSKI
  B. ZANFAGNA

- CHAUFFAGE CYCLOTRONIQUE IONIQUE..... J. ADAM
  P. BANNELIER
  R. BRUGNETTI
  D. GAMBIER
  H. KUUS

INFORMATIQUE

- MATÉRIEL..... M. CHARET
- LOGICIEL..... J. BRETON
  A. COGEN
  C. REVERDIN
  J. TOUCHE

THÉORIE ..... J. ANDREOLETTI
  H. CAPES
  M. DUBOIS
  I. FIDONE
  G. GIRUZZI
  V. KRIVENSKI
  M. PAIN
  A. SAMAIN